Giant magnetoresistance in sputtered $(Co_{70}Fe_{30})_xAg_{1-x}$ heterogeneous alloys

1994 J. Phys.: Condens. Matter 6 5545

(http://iopscience.iop.org/0953-8984/6/28/026)

J. Phys.: Condens. Matter 6 (1994) 5545–5560. Printed in the UK

Giant magnetoresistance in sputtered $(Co_{70}Fe_{30})_xAg_{1-x}$ heterogeneous alloys

S R Teixeira†§, B Dieny†, A Chamberod†, C Cowache†, S Auffret†, P Auric†, J L Rouvière†, O Redon‡ and J Pierre‡

† CEA, Département de Recherche Fondamentale sur la Matière Condensée, 38054 Grenoble Cédex 9, France

‡ Laboratoire Louis Néel, CNRS, BP166X, 38042 Grenoble Cédex, France

Received 22 November 1993, in final form 2 February 1994

Abstract. We report the structural, magnetic and transport properties of $(Co_{70}Fe_{30})_xAg_{1-x}$ heterogeneous alloys, with x varying between 27 and 47 at.%. The samples were prepared by DC triode sputtering at room temperature (RT) and liquid-nitrogen temperature. Annealing processes lead to phase segregation and grain growth, resulting in the formation of small and compact $Co_{70}Fe_{30}$ precipitates. The resulting evolution of the magnetic properties has been investigated by SQUID magnetometry, Mössbauer spectroscopy and ferromagnetic resonance. The largest magnetoresistance amplitudes at room temperature have been obtained for a magnetic concentration x of around 36 at.% in both as-deposited and annealed samples. Amplitudes $\Delta R/R(H = 0)$ of 15% in the as-deposited samples and 21% in samples annealed at 600 K for 10 min have been observed at RT. At 4 K these amplitudes reach 43% (equivalent to $\Delta R/R(H = 2\ \mathrm{T}) = 75\%$).

1. Introduction

The recent discovery of giant magnetoresistance (GMR) in magnetic granular alloys [1,2] has added a new dimension to the phenomenon of GMR in magnetic multilayers. These granular alloys consist of ultra-fine ferromagnetic particles embedded in an immiscible medium. Examples of alloys in which GMR has been observed include Co_xCu_{1-x} [1,2], Co_xAg_{1-x} [3–11], $NiFe_xAg_{1-x}$ [11,12] and Fe_xAg_{1-x} [10,11]. GMR in multilayers and granular alloys has a common origin. It is related to a change in the magnetic arrangements of the moments of the magnetic layers or particles when a magnetic field is applied. The resistivity is at a minimum when the moments of the magnetic entities are parallel to each other, i.e. at saturation. It increases as this parallel alignment becomes more and more perturbed (this occurs when the field decreases to zero or at a coercive field). It is well established that the main origin of GMR is the spin-dependent scattering of conduction electrons occurring at the interfaces and/or in the bulk of the ferromagnetic entities. Fairly large GMR amplitudes have been obtained in granular alloys, especially at low temperatures [2,5,6,10–12]. In optimized systems, GMR amplitudes may be larger than in multilayers, since granular systems represent an intermediate situation between current-in-plane (CIP) and current-perpendicular-to-the-plane (CPP) configurations [13] in magnetic multilayers. Saturation fields in granular alloys are still too large for low-field applications, in particular

§ Permanent address: Instituto de Fisica, Universidade Federal do Rio Grande do Sul, 91501-970, Porto Alegre, RS, Brazil.

0953-8984/94/285545+16$19.50

in magnetic recording technology. However, applications of these systems at higher fields can be foreseen (for instance in the car industry). Furthermore, attempts to reduce the saturation fields are still in progress [14].

In this paper we present an experimental study of structural, magnetic and transport properties of a series of $(Co_{70}Fe_{30})_xAg_{1-x}$ granular alloys (x varying between 27 and 47 at.%) prepared by sputtering. It has been shown that $Co_{1-x}Fe_x$/Cu multilayers with an Fe concentration in Co of the order of 10–30 at.% exhibit magnetoresistance (MR) ratios larger than those of Co/Cu multilayers [15]. It was therefore an aim of this work to see whether a similar MR enhancement occurs in this series in comparison with sputtered Co_xAg_{1-x}.

2. Experimental details

We used a triode DC sputtering system with two independent targets (50 mm diameter, one consisting of a $Co_{70}Fe_{30}$ alloy, and the other of Ag) operating at different powers. The two targets were tilted such that the sputtered species were directed towards the substrate holder. The films were deposited on glass substrates at room temperature (RT) and liquid-nitrogen (LN_2) temperature (77 K). The base pressure was 5×10^{-8} Torr, while sputtering was carried out in an Ar atmosphere of 0.8×10^{-3} Torr. Several glass substrates (3 mm by 25 mm) were fixed parallel to each other on the substrate holder (70 mm diameter). Owing to the geometry of our system, the flux from each target was not uniform over the substrate holder but rather showed an overall inhomogeneity of about 20%. As a result, when cosputtering of $Co_{70}Fe_{30}$ and Ag was performed from the two targets, a concentration gradient was obtained across the series of substrates. This allowed for the preparation of 14 samples of various compositions in the same run. The inhomogeneity in magnetic concentration over each sample (3 mm wide) is of the order of 1 %. The total thickness of the films was about 1 μm. The concentration of the magnetic species ($Co_{70}Fe_{30}$), measured by electron dispersion spectroscopy using a JEOL-JSM-840A scanning microscope, showed a variation between 27 and 47 at.% along the series of substrates. The crystallographic structure of the samples was investigated by conventional θ–2θ x-ray diffraction using Co Kα radiation and by transmission electron microscopy (TEM) using JEOL 200CX and JEOL 4000EX microscopes. For TEM observations, classical cross sections thinned by argon ion milling were used. The temperature of the sample can rise to about 400 K during the thinning process. For samples prepared at 77 K, which are highly metastable, this rise in temperature leads to a significant structural evolution of the film. Therefore reliable conclusions could not be derived from TEM observations on these as-deposited samples prepared at 77 K. For samples prepared at RT, measurements of electrical resistivity during annealing indicates that little structural evolution occurs up to 400 K so that the thinning process should not affect the structure of the film.

Magnetic moment measurements were performed with a SQUID magnetometer in the ranges 0–6 T and 1.5–300 K. The local magnetic properties of the Fe atoms were investigated by Mössbauer spectroscopy in transmission geometry at RT in zero field, using a 100 mCi ^{57}Co source in a Rh matrix. Electrical resistivity measurements were performed using a four-point probe and a lock-in amplifier in the AC mode in the ranges 4–300 K and 0–6 T.

3. Results and discussion

3.1. Structural properties

In order to explain the essential features of the structural properties, we present here the results obtained for heterogeneous alloys containing 36 at.% of $Co_{70}Fe_{30}$. This composition is of particular interest in this series since it gives the largest MR amplitude of all the compositions investigated (see figure 9). Detailed x-ray measurements and TEM observations were made on samples of this particular composition.

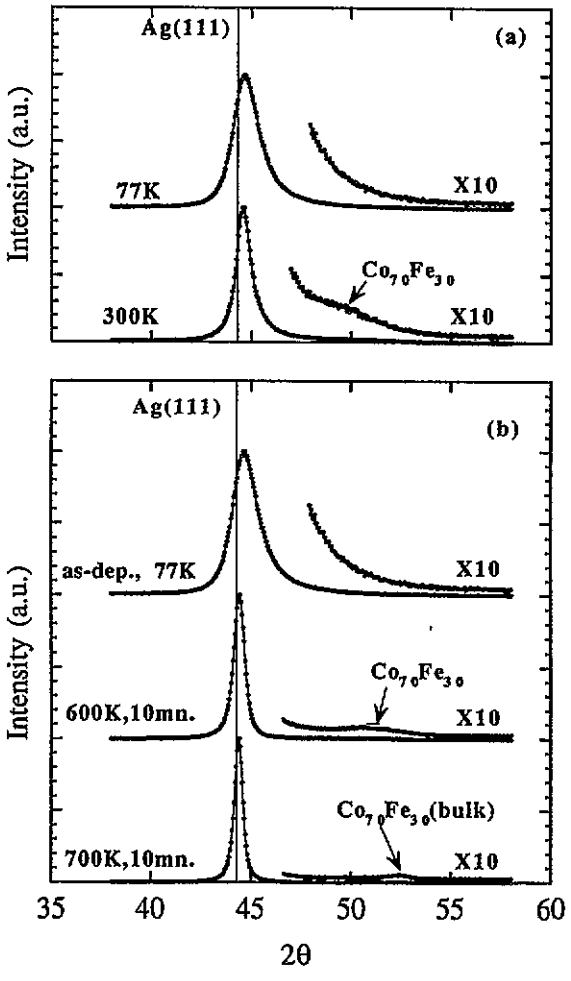

Figure 1. (*a*) Comparison of θ–2θ x-ray spectra of two samples of the composition $(Co_{70}Fe_{30})_{36}Ag_{64}$ prepared at LN_2 temperature and RT, respectively (a.u. arbitrary units). (*b*) X-ray spectra of the same sample (prepared at LN_2 temperature) in the as-deposited state and after two successive anneals for 10 min at 600 and 700 K (a.u. arbitrary units).

Figure 1(*a*) shows the x-ray spectra for samples deposited at 77 and 300 K. Only ⟨111⟩ lines are visible for FCC Ag when 2θ is scanned between 40° and 120°, indicating that the as-deposited samples have a pronounced ⟨111⟩ texture. The vertical line in figure 1 indicates the expected position of the diffraction peak for bulk Ag(111). The position of the Ag(111) peak in the actual sample is shifted towards larger angles, indicating either compressive strains in the Ag lattice or the existence of a solid solution of Co and Fe in Ag. In the samples deposited at 77 K, the magnetic atoms are very finely dispersed in the Ag matrix since absolutely no hint of $Co_{70}Fe_{30}$ peaks is observed in the spectrum. A metastable

alloy has been formed in which the Co and Fe atoms are almost randomly distributed in the Ag polycrystalline matrix. In contrast with this, samples deposited at 300 K possess a shoulder which can be seen in the amplified part of the spectrum, indicating the formation of $Co_{70}Fe_{30}$ precipitates. The size of these precipitates estimated from TEM observations (see later) is nevertheless smaller than 10 Å. For both deposition temperatures, the Ag(111) peaks are quite broad, which indicates small grain sizes, non-uniform strains or inhomogeneous alloying between $Co_{70}Fe_{30}$ and Ag on the atomic scale. The peaks in the x-ray spectra are nevertheless narrower for samples deposited at 300 K (larger grains and better segregation between $Co_{70}Fe_{30}$ and Ag during deposition) than for samples deposited at LN_2 temperature.

Figure 1(*b*) shows x-ray spectra of a sample deposited at 77 K after two successive annealing treatments at 600 and 700 K for 10 min. The spectrum of the as-deposited sample is shown at the top of the figure for comparison. The vertical scale on the right-hand side of the spectra is expanded for clarity. Owing to the high metastability of the as-deposited samples, a large structural evolution occurs upon annealing. A progressive increase in the $Co_{70}Fe_{30}$ peak clearly appears in figure 1(*b*). The Ag(111) and $Co_{70}Fe_{30}$ peaks become narrower and shift progressively towards their respective bulk values. These effects are due to a progressive segregation between Ag and $Co_{70}Fe_{30}$ which leads to grain growth and strain relaxation and to an overall improvement in the crystallographic structure. The upper limit of the grain sizes estimated from the width of the lines after annealing at 700 K for Ag and $Co_{70}Fe_{30}$ are 210 Å and 70 Å, respectively. Even after annealing at this temperature, only reflections in ⟨111⟩ directions were observed, indicating that the texture of the films remained unaltered.

TEM observations confirmed the x-ray results and provide additional information about the crystallography and grain size. Two samples have been investigated. One was an as-deposited sample of the composition $(Co_{70}Fe_{30})_{36}Ag_{64}$ prepared at 300 K. The other, of the same composition, was prepared at 300 K and annealed at 700 K for 10 min.

Figure 2 provides a qualitative comparison of the texture of these two samples. The diffraction patterns of the samples are shown in figures 2(*c*) and 2(*d*). For both samples, Ag spots were observed, confirming the ⟨111⟩ texture determined by x-ray diffraction. The spots associated with the diffraction by the magnetic precipitates were hardly visible. In the annealed sample, clear Ag diffraction spots and fainter $Co_{70}Fe_{30}$ spots, visible in the diffraction pattern in figure 2(*d*), show the good crystallography of the sample. Dark-field images (figures 2(*a*), 2(*b*) and 3) have been obtained by selecting particular spots in the diffraction patterns. The selected spots are respectively associated with the following characteristics (figure 2(*d*)):

position A: selection of all Ag and $Co_{70}Fe_{30}$ grains having a ⟨111⟩ texture;

position B: selection of one family of ⟨111⟩ textured Ag and $Co_{70}Fe_{30}$ grains seen along one particular ⟨011⟩ direction;

position C: selection of some $Co_{70}Fe_{30}$ precipitates having a ⟨111⟩ texture.

Figures 2(*a*) and 2(*b*) are dark-field images of the two samples taken with the aperture in position A. The white parts on the figure come from Ag and $Co_{70}Fe_{30}$ grains having a ⟨111⟩ texture. This texture is visible in the as-deposited sample (figure 2(*a*)) but is clearly more pronounced in the annealed sample (figure 2(*b*)). The morphology of the sample deposited at RT looks granular. In the annealed sample (figure 2(*b*)), a large improvement in the crystallographic structure is observed. Strong moiré contrasts are seen corresponding to a multiple diffraction of the electrons by the Ag and $Co_{70}Fe_{30}$ grains. Such moiré contrasts are not seen in the former samples in which the $Co_{70}Fe_{30}$ precipitates are too small to be visible (less than 10 Å). A columnar structure of the annealed sample can already be seen in figure 2(*b*). It appears much more clearly in figure 3(*b*) with the aperture in position B.

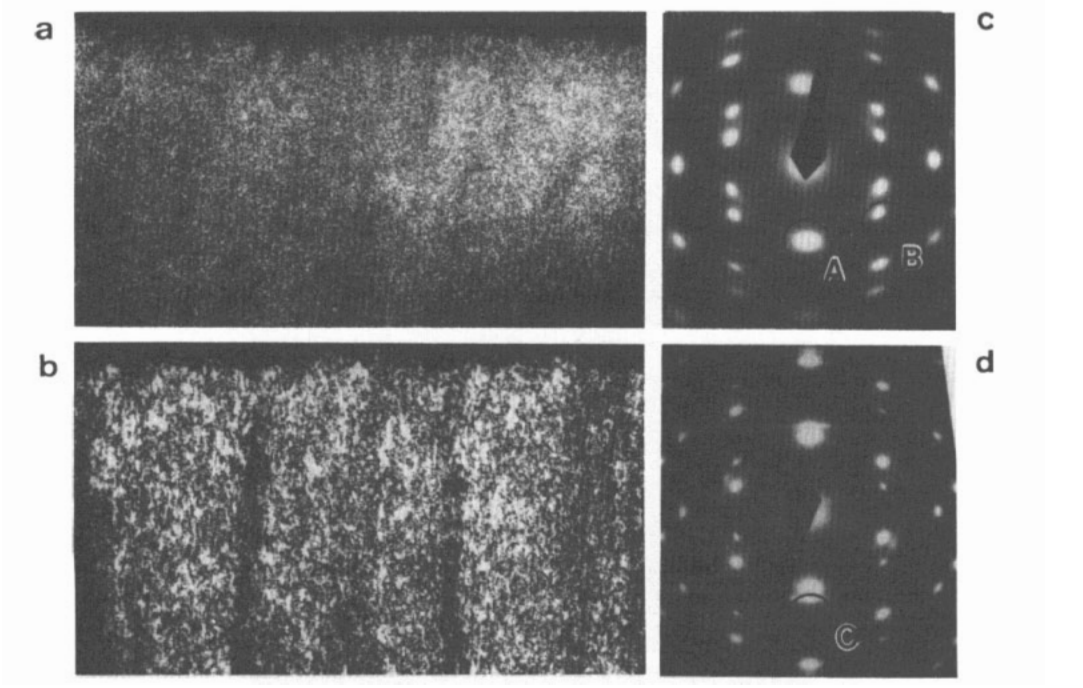

Figure 2. (*a*), (*b*) Dark-field images of as-deposited samples (*a*) prepared at 300 K and (*b*) annealed at 700 K (after preparation at 77 K) for 10 min, with the aperture at position A of the diffraction pattern. (*c*) (*d*) Corresponding diffraction patterns. The different positions of the aperture used in the TEM dark-field observations are indicated in (*c*) and (*d*).

Figures 3(*a*) and 3(*b*) illustrate the improvement in the columnar structure of the samples upon annealing. These dark-field images have been taken with the aperture in position B. The white parts correspond to a family of (111) textured grains viewed along a particular (011) direction. In the as-deposited sample (prepared at RT) (figure 3(*a*)) a tendency towards a columnar structure is observed. However, the columns are rather narrow (100–400 Å) and do not extend throughout the deposited layer. After annealing at 700 K for 10 min (figure 3(*b*)), a large improvement in this columnar structure is observed. The contrast between neighbouring columns is much more pronounced and they extend over much larger distances. In each column, silver is crystalline and keeps the same orientation to within a few degrees. The columns may be considered to be either single crystals with a large density of structural defects (these defects include the cobalt–iron precipitates) or families of small adjacent grains having approximately a common orientation. The diameters of the columns range from 200 to 700 Å.

In figure 3(*c*), a family of $Co_{70}Fe_{30}$ precipitates has been selected with the aperture in position C. The location of these precipitates corresponds to the moiré contrasts observed in figure 2(*b*). In this annealed sample, the magnetic precipitates look rather compact. They have an almost round shape and their sizes range between 20 and 60 Å. They could not be observed in the as-deposited samples because of their excessively small size (less than 10 Å). The crystallographic orientation of these precipitates is coherent with the local orientation of the Ag matrix since they follow the columnar structure of the matrix. The resolution is not high enough to determine whether the magnetic precipitates are entirely

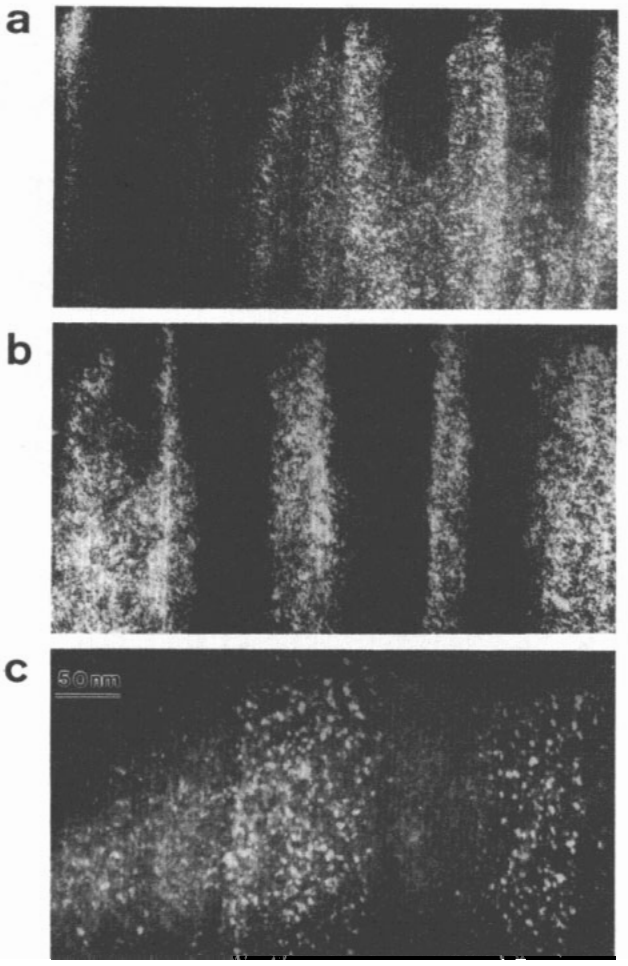

Figure 3. (*a*), (*b*) Dark-field images of (*a*) the as-deposited sample (prepared at 300 K) and (*b*) after annealing at 700 K for 10 min (aperture at position B in figure 2(*c*)). (*c*) Dark-field image of the $Co_{70}Fe_{30}$ precipitates in the same annealed sample as (*b*) (aperture at position C in figure 2(*d*)).

coherent with the matrix (i.e. no interfacial dislocations) or whether they are only partially coherent (the presence of interfacial dislocations). However, in a comparable series of alloys, $NiFe_xAg_{1-x}$, we did observe, with an atomic resolution, that the Ag matrix contains a large density of structural defects. In fact, a strong relaxation occurred via the formation of dislocations around the magnetic grains [12]. A similar nanostructure probably exists in the present series of alloys.

3.2. Magnetic properties

Figure 4(*a*) shows the magnetization curves $M(H)$ of an as-deposited sample of the composition $(Co_{70}Fe_{30})_{36}Ag_{64}$ prepared at 77 K, and figures 4(*b*) and 4(*c*) those after two successive anneals at 700 K and 900 K, respectively, for 10 min. The data are expressed in electromagnetic units per cubic centimetre of film. Two main results must be emphasized.

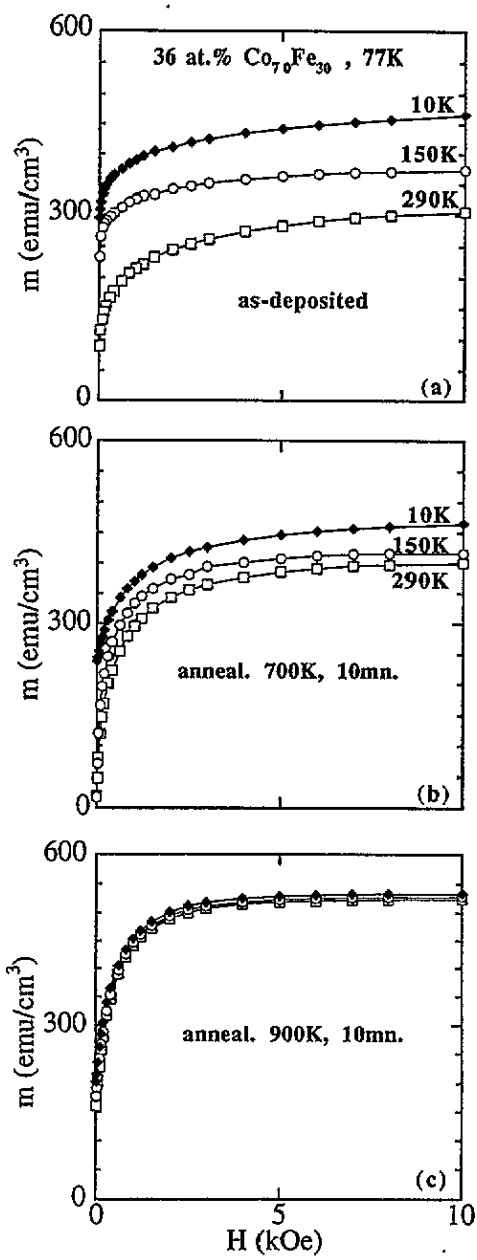

Figure 4. Magnetization curves measured at various temperatures of (*a*) an as-deposited sample of the composition $(Co_{70}Fe_{30})_{36}Ag_{64}$, (*b*) of the same sample after annealing at 700 K for 10 min and (*c*) of the same sample after further annealing at 900 K for 10 min.

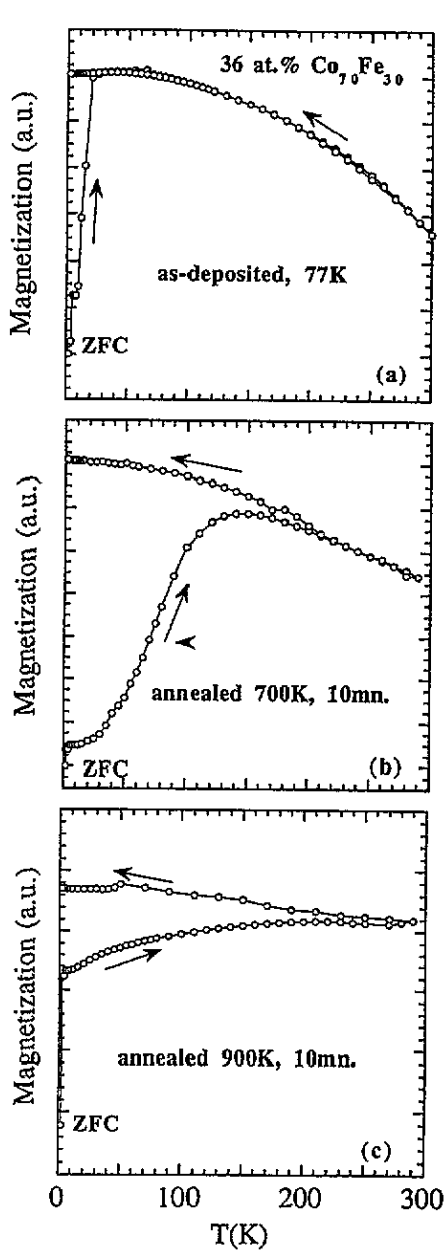

Figure 5. ZFC and FC (at 40 Oe) thermal variation in the magnetization of (*a*) an as-deposited sample of the composition $(Co_{70}Fe_{30})_{36}Ag_{64}$ (prepared at 77 K), (*b*) of the same sample after annealing at 700 K for 10 min and (*c*) of the same sample after further annealing at 900 K for 10 min (a.u. arbitrary units).

The first point concerns the behaviour of the remnant magnetization above 150 K. The remnant magnetization is rather large in the as-deposited sample. It drops to almost zero after the first anneal at 700 K but increases after a further anneal at 900 K. This behaviour contrasts

with that observed for the Co–Cu, Fe–Ag [11] and $NiFe_xAg_{1-x}$ series [12]. For this latter series, in the range of compositions for which $x < 25$ at.% ($x = 25$ at.% is the composition for which the largest MR is obtained), the as-deposited samples are superparamagnetic at RT. Upon annealing, a large enhancement in the ferromagnetic contribution to the magnetization occurs. The opposite tendency observed in $(Co_{70}Fe_{30})_xAg_{1-x}$ between the as-deposited and the annealed samples is probably related to the change in the nanostructure of the $Co_{70}Fe_{30}$ precipitates upon annealing. The magnetic part of the as-deposited samples consists of small ferromagnetic cores rich in Co and Fe surrounded by a ramified envelope of $(Co_{70}Fe_{30})_xAg_{1-x}$ alloy. These ramifications act as magnetic bridges between $Co_{70}Fe_{30}$ particles, leading to a largely ferromagnetic behaviour of the system. Upon annealing, $Co_{70}Fe_{30}$ tends to coalesce, forming more compact precipitates. The magnetic bridges between particles are broken so that the magnetic precipitates become superparamagnetic at RT. Further annealing (at 900 K for 10 min) leads to an increase in the size of magnetic precipitates and correlatively to an increase in the blocking temperature (reinforcement of the ferromagnetic behaviour) as observed in the $NiFe_xAg_{1-x}$ series [12] (see also figure 5(*c*) later). The increase in remnant magnetization in figure 4(*c*) is due to the more hysteretic behaviour of these blocked precipitates.

The second point concerns the thermal variation in the magnetization of the as-deposited and annealed samples. The magnetization curves are much more temperature dependent for the as-deposited sample than for the annealed samples. The higher the annealing temperature, the weaker is the temperature dependence of the magnetization. In the as-deposited sample prepared at 77 K, the magnetic species are dispersed in very fine and ramified particles (size smaller than 10 Å). The large temperature dependence of the magnetization observed in figure 4(*a*) is due to the thermal activation of these ramified and interconnected particles. Upon annealing, as discussed above, the Co and Fe atoms coalesce, leading to the disappearance of these tiny precipitates. As the size of the magnetic precipitates increases, the magnetization processes become more and more determined by a balance between the applied field and the shape anisotropy of each grain or couplings between grains (magnetostatic or RKKY). The temperature no longer influences the magnetization curves (figure 4(*c*)). At low temperatures, some hysteresis appears. The coercive field is of the order of 500 Oe at 4 K. This hysteresis also appears in the MR curve (see figure 12 later).

Figures 5(*a*)–5(*c*) show the zero-field-cooled (ZFC) and field-cooled (FC) (in 40 Oe) magnetization curves $M(T)$ for the same samples as in figures 4(*a*)–4(*c*). In the as-deposited sample, a completely reversible $M(T)$ variation is observed above 20 K. The very rapid increase in the ZFC magnetization between 1.5 and 20 K is consistent with the large remnant magnetization observed at low temperatures in the magnetization curve (figure 4(*a*)). In the range 10–20 K, a field of 40 Oe is sufficient to induce a magnetization in the system corresponding to three fifths of its value in 10 kOe (figure 4(*a*)). Above 20 K, the observed reversible decay of the magnetization is mainly due to the alteration of this low-field magnetization by thermal activation. Extrapolating the $M(T)$ variation between 30 and 400 K leads to an estimate for the Curie temperature of 380 K, which is much lower than that of pure Co or pure Fe. This reduction in T_C is due to alloying between Ag and $Co_{70}Fe_{30}$ and to a finite size effect.

After annealing at 700 K (figure 5(*b*)), a large thermal hysteresis is observed below 200 K. The $M(T)$ and $M(H)$ curves (figure 4(*b*)) indicate superparamagnetic behaviour above 230 K. The broad distribution of blocking temperatures is associated with the distribution of the size of the superparamagnetic clusters. The upper limit of this distribution (which corresponds to the largest clusters) is given by the temperature at which the ZFC

curve becomes reversible (230 K in figure 5(*b*)). The Curie temperature in the annealed samples has significantly increased in comparison with that of the as-deposited samples. After the second anneal (figure 5(*c*)), the blocking temperature has increased above RT. The thermal variation in magnetization between 300 and 1.5 K (FC curve) becomes comparable with that of the bulk $Co_{70}Fe_{30}$ alloy.

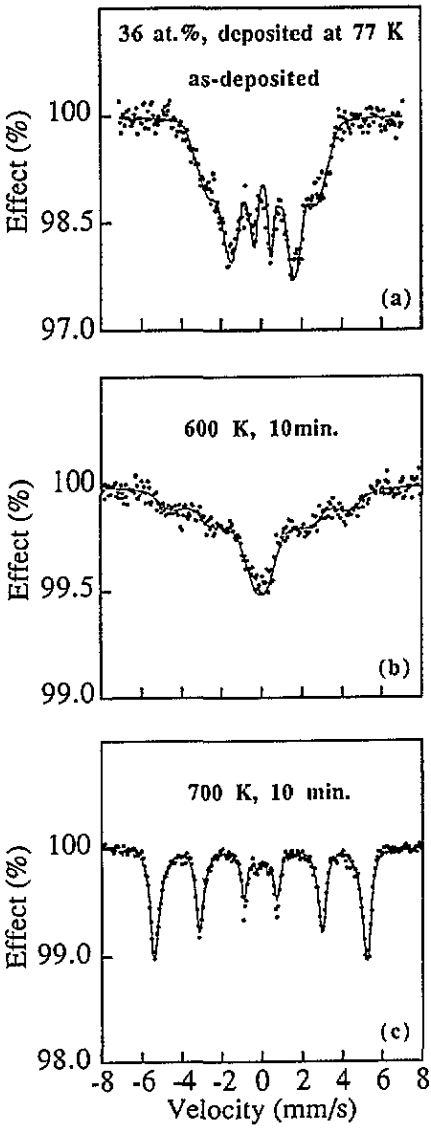

Figure 6. Mössbauer spectra at room temperature of (*a*) an as-deposited sample of the composition $(Co_{70}Fe_{30})_{36}Ag_{64}$, (*b*) of the same sample after an anneal at 600 K for 10 min and (*c*) of the same sample after a second anneal at 700 K for 10 min.

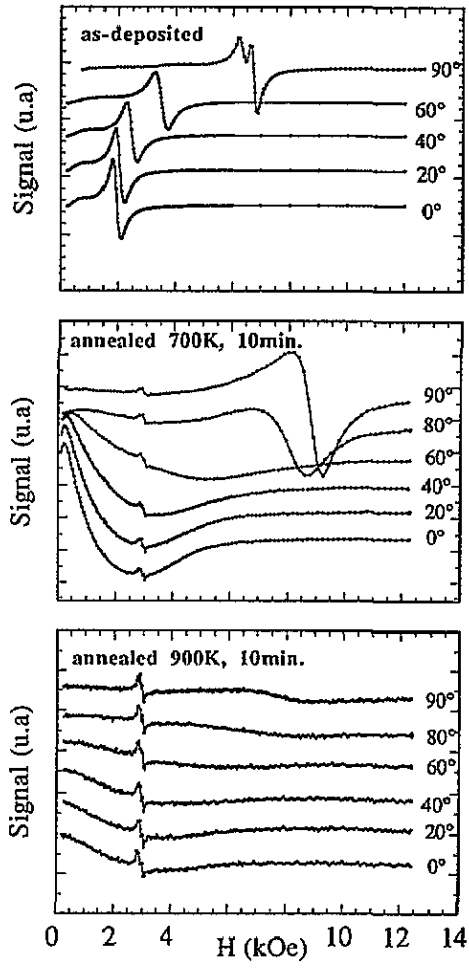

Figure 7. Ferromagnetic resonance spectra measured at RT and 9.7 GHz of (*a*) an as-deposited sample of the composition $(Co_{70}Fe_{30})_{36}Ag_{64}$, (*b*) of the same sample after annealing at 700 K for 10 min and (*c*) of the same sample after further annealing at 900 K for 10 min (same conditions as in figures 4 and 5) (a.u. arbitrary units).

Figure 6(*a*) shows the Mössbauer spectrum obtained at RT for the same as-deposited sample as in figures 4 and 5 (36 at.% $Co_{70}Fe_{30}$ prepared at 77 K). The spectra in figures 6(*b*) and 6(*c*) correspond to the same sample after annealing at 600 K and 700 K, respectively, for 10 min. The parameters deduced from the fits of the spectra are collected in table 1. The spectrum of the as-deposited sample shows the superposition of a paramagnetic contribution (which comes from the Fe atoms which are the most finely dispersed within the Ag matrix) and a ferromagnetic contribution. The spectrum associated with this latter contribution is characterized by a broad linewidth and low values of the hyperfine fields. These features are typical of amorphous Fe alloys and are consistent with the very fine dispersion of the magnetic species in the Ag matrix observed by TEM. The Fe moments lie approximately in the plane of the film, probably because of the overall shape anisotropy of the sample.

Table 1. Hyperfine parameters corresponding to Mössbauer spectra measured at 300 K (figure 6). The non-magnetic contribution is related to isolated Fe atoms or to Fe atoms in a paramagnetic environment. The magnetic contribution was fitted with a hyperfine field distribution correlated with an isomer shift distribution. $\langle IS \rangle$ and $\langle H \rangle$ are the mean value of the isomer shifts relative to Fe in Rh and the hyperfine fields, respectively. θ_0 is the mean angle between the hyperfine field direction and the normal of the film plane.

		Value for the following samples		
Sample	Parameter (units)	As deposited	Annealed at 600 K	Annealed at 700 K
Non-magnetic	(%)	13.4	45.0	3.9
	$\langle IS \rangle$ (mm s^{-1})	0.040	−0.039	−0.020
	QS (mm s^{-1})	0.90	0.40	0.48
	Γ (mm s^{-1})	0.74	1.35	0.24
Magnetic	(%)	86.6	55.0	96.1
	$\langle IS \rangle$ (mm s^{-1})	0.074	−0.050	−0.110
	$\langle H \rangle_n$ (T)	15.8	22.2	32.4
	H_{min}–H_{max}	4.9 → 23.2	10.1 → 33.3	29.3 → 34.3
	θ_0 (deg)	70	54	54
	Γ (mm s^{-1})	0.32	0.66	0.31

After the first anneal at 600 K, a large modification is observed in the spectrum (figure 6(*b*)). The paramagnetic contribution has significantly increased while the ferromagnetic part has been reduced. This is consistent with the SQUID measurements (figure 4) which show a decrease in remnant magnetization upon moderate annealing. This effect has been interpreted as being caused by a decoupling of the $Co_{70}Fe_{30}$ precipitates due to the disappearance of the magnetic bridges between grains as discussed above (figures 4(*a*) and 4(*b*)).

After further annealing (700 K for 10 min), the spectrum indicates quite a dominant ferromagnetic behaviour, although a small paramagnetic contribution remains. The hyperfine field H_{hf} is no longer distributed (see table 1), indicating a well crystallized nanostructure of $Co_{70}Fe_{30}$ grains. The values of H_{hf} are the same as in bulk $Co_{70}Fe_{30}$ alloys [16]. It should be pointed out that the blocking temperature for Mössbauer measurements (characteristic time of 10^{-8} s) is about 3 times the blocking temperature for SQUID measurements (characteristic time of 1 s). This explains why the sample annealed at 700 K appears ferromagnetic from Mössbauer data (figure 6(*a*)) and superparamagnetic from SQUID data (figure 4(*b*)). Furthermore, in the annealed sample, the Fe moments lie at an average angle of 54° from the normal to the film plane (see table 1) which in fact indicates an isotropic distribution of these moments.

Ferromagnetic resonance (FMR) (at 9.7 GHz) measurements (figure 7) at RT have been carried out on the same as-deposited and annealed samples as those used for the SQUID measurements (figures 4 and 5). For each sample, a series of spectra has been collected corresponding to various orientations of the applied field with respect to the plane of the film (from 0° (in-plane configuration) to 90° (perpendicular configuration)). For the as-deposited sample, a typical ferromagnetic line is observed which shifts towards larger resonance fields as the sample is rotated from the in-plane to perpendicular configurations. Such a shift indicates an overall in-plane anisotropy which is consistent with the Mössbauer results. The in-plane anisotropy field $4\pi M_s - H_a$ can be estimated from the shift of the resonance lines between 0 and 90°. On the assumption that the magnetic species form a continuous thin film, the resonance fields in the plane of the film are perpendicular to the plane given by [17]

$$H_{\parallel} = \frac{1}{2}\left[-(4\pi M_s - H_a) + \sqrt{(4\pi M_s - H_a)^2 + 4\left(\frac{\omega}{\gamma}\right)^2}\right]$$

and

$$H_{\perp} = (4\pi M_s - H_a) + \frac{\omega}{\gamma}.$$

Taking the experimental values $H_{\parallel} = 2000$ Oe, $H_{\perp} = 6700$ Oe and $\omega/\gamma = 3220$ Oe, one finds that $4\pi M_s - H_a = 3500$ Oe. Furthermore, the magnetization of this sample of around 6 kOe at RT is of the order of 270 emu cm^{-3} (see figure 4(*a*)). This leads to $4\pi M_s \simeq 3400$ Oe and therefore $H_a \simeq -100$ Oe. This indicates that the main contribution to the in-plane anisotropy in this sample is simply the overall shape anisotropy of the film.

After annealing at 700 K (figure 7(*b*)), three lines are observed:

(i) a ferromagnetic line which is mainly visible when the applied field is perpendicular to the plane of the sample;

(ii) a paramagnetic line which does not shift when the sample is rotated (resonance field equal to $\omega/\gamma = 3200$ Oe). This line can be ascribed to a very small paramagnetic clustering of $Co_{70}Fe_{30}$;

(iii) a line at very low fields which is mainly visible when the field is applied in the plane of the sample (such a low-field line has already been observed in the FMR spectra of $NiFe_xAg_{1-x}$ granular alloys [12] and has been ascribed to the incoherent precession of supermagnetic clusters).

Therefore the present results are consistent with an increase in the superparamagnetic contribution to the magnetization of the sample after the first anneal. The width of the ferromagnetic line has significantly increased in comparison with figure 7(*a*). Correlatively, its intensity has decreased (the gain of the detector is larger in figure 7(*b*) than in figure 7(*a*)). This increase in the width of the line indicates a broadening in the distribution of the internal field which is probably associated with a large distribution in the size and shape of the magnetic particles (consistent with the isotropic distribution of Fe moments observed by Mössbauer spectroscopy in annealed samples).

After the second anneal, the intensity of the ferromagnetic line has again decreased because of further broadening in the distribution of the internal field acting on the magnetic precipitates. The internal field becomes more and more widely distributed, probably because of the increase in the role of the shape anisotropy of the individual magnetic grains and

of the magnetostatic coupling between particles. The fact that the blocking temperature of this sample is very close to room temperature (see figure 5(*c*)) may also lead to an amplification in the inhomogeneity of the internal field acting on the magnetic clusters. A small paramagnetic line is still present, indicating that, despite the high annealing temperature, a small fraction of the magnetic species is still dispersed in the Ag matrix.

3.3. Transport properties

3.3.1. Electrical resistivity. The electrical resistivity of the as-deposited samples is plotted in figure 8(*a*) versus the concentration of magnetic species. The resistivity of the samples deposited at 77 K is about 50% larger than the resistivity of those deposited at RT. This is consistent with the higher degree of structural disorder of the samples prepared at LN_2 temperature observed by x-ray diffraction and TEM studies. The resistivity of these alloys (measured at 16 kOe) almost does not depend on the magnetic concentration. It is of the order of 40 $\mu\Omega$ cm for the samples prepared at 77 K, compared with 27 $\mu\Omega$ cm for the samples prepared at RT. This may indicate that increasing the magnetic concentration does not change the density of $Co_{70}Fe_{30}$–Ag interfaces very much but instead leads to an increase in the size of the magnetic precipitates. It is interesting to note that the resistivity in zero field shows a maximum at around 35 at.% $Co_{70}Fe_{30}$ owing to the magnetoresistance which leads to an increase in resistivity at low fields (for a larger magnetic disorder, see below).

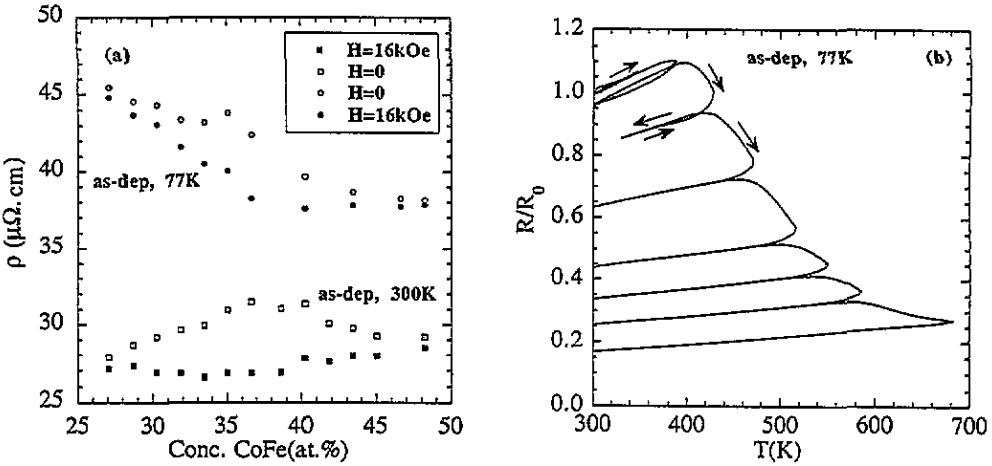

Figure 8. (*a*) Variation in the resistivity at RT and 0 and 16 kOe versus $Co_{70}Fe_{30}$ atomic concentration for two series of samples prepared at LN_2 temperature and RT. (*b*) Variation in the resistivity of a sample of the composition $(Co_{70}Fe_{30})_{36}Ag_{64}$ upon annealing. The temperature is scanned up and down between RT and an increasingly high temperature at a rate of 2 K min^{-1}.

Figure 8(*b*) shows the evolution of the resistivity upon annealing for the sample of concentration 36 at.% $Co_{70}Fe_{30}$. In this experiment, the temperature was scanned up and down at a rate of 2 K min^{-1} between RT and an increasingly high temperature. As already observed for the $NiFe_xAg_{1-x}$ series [12], the variation in the resistivity exhibits two types of behaviour: reversible variations associated with phonon and magnon scattering and an irreversible decrease associated with the structural evolution of the alloy. The structural evolution involves a demixing between $Co_{70}Fe_{30}$ and Ag, an increase in the size of the

$Co_{70}Fe_{30}$ and Ag grains, an increase in the size of the crystallites and a decrease in the density of crystallographic defects (grain boundaries and dislocations). The resulting relative drop in resistivity ρ is quite large (a factor of 5).

3.3.2. Magnetoresistance. The results of MR measurements are shown in figure 9. Figure 9(*a*) shows the MR amplitude $[R(H_{max} = 16\ kOe) - R(0)]/R(0)$ of two series of as-deposited samples prepared at 300 and 77 K versus the $Co_{70}Fe_{30}$ content. The MR shows a peak for both series at 36 at.% $Co_{70}Fe_{30}$. This value is quite different from the values obtained for Fe–Ag, NiFe–Ag and Co–Cu heterogeneous alloys [2]. the magnetic concentration at which this maximum occurs corresponds to a threshold above which ferromagnetic couplings between grains become too large and prevent the necessary change in the relative orientation of magnetizations in neighbouring grains from random in zero field to parallel at saturation. The fact that this threshold occurs at higher magnetic concentrations than in the other series of alloys indicates a more compact shape of the magnetic precipitates in the as-deposited samples. This may be ascribed to the larger immiscibility of Co in Ag than of Co in Cu or of Ni in Ag [18]. In other respects, the increase in the MR at low increasing magnetic concentration is ascribed to the increasing density of spin-dependent scattering centres and correlates to a decrease in the shunting effect through the Ag matrix.

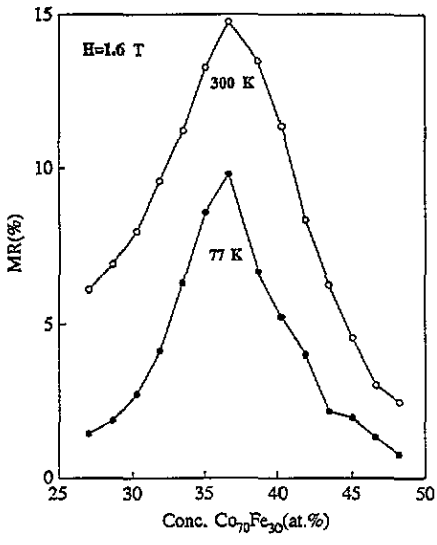

Figure 9. Variation in the MR amplitude at RT (GMR between 0 and 16 kOe) versus $Co_{70}Fe_{30}$ atomic concentration for two series of samples prepared at LN_2 temperature and RT.

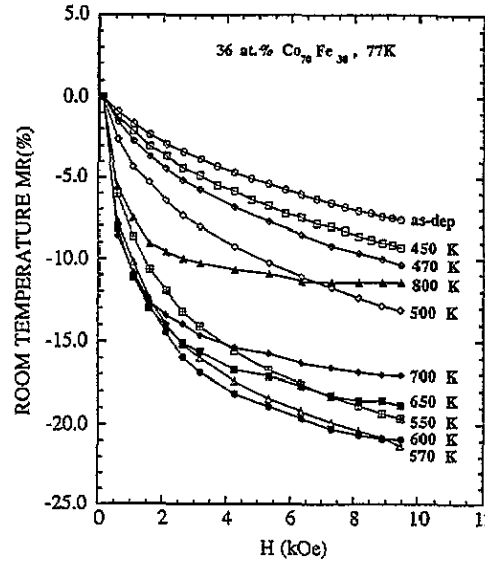

Figure 10. MR curves measured at RT between 0 and 16 kOe for a sample of the composition $(Co_{70}Fe_{30})_{36}Ag_{64}$ after successive anneals for 10 min at various temperatures.

The larger MR amplitude observed for samples deposited at RT in comparison with those deposited at 77 K may be ascribed to their different nanostructures. In the samples prepared at 77 K, the magnetic species are almost randomly distributed in the Ag matrix while, in those prepared at RT, small $Co_{70}Fe_{30}$ precipitates can be observed. This is confirmed by the difference in their resistivities (60 $\mu\Omega$ cm for the sample with 36 at.% $Co_{70}Fe_{30}$ prepared at 77 K compared with 40 $\mu\Omega$ cm for the samples prepared at RT).

The effect of the annealing temperature on the MR is illustrated in figure 10 for samples with 36 at.% $Co_{70}Fe_{30}$ prepared at 77 K. All successive anneals had a duration of 10 min. the MR amplitude first increases with increasing annealing temperature and reaches a maximum after annealing at 570 K for 10 min. At this stage, the size of the magnetic precipitates, estimated from TEM observation, is distributed between 15 and 50 Å.

As already observed for the $(NiFe)_xAg_{1-x}$ series [12], the MR curves consist of a rather steep decrease in low fields followed by a tail at high fields. The initial decrease in resistivity has the same physical origin as the GMR in magnetic multilayers. It is associated with the rotation of the magnetizations of the grains in the direction of the field. In contrast, the long MR tail at high fields is ascribed to a progressive saturation of the paramagnetic or superparamagnetic fluctuations. Note that the variation in the slope of the MR curves at large fields (above 8 kOe) with the annealing temperature (an increase in the slope up to an intermediate temperature of about 550 K and a decrease above) is consistent with the discussion of the magnetic results (an initial increase in the superparamagnetic contribution to the magnetization up to an intermediate annealing temperature and then a decrease for higher annealing temperatures).

The MR amplitudes observed at RT in this series of alloys are fairly large ($\Delta R/R(H = 0) = 20\%$ equivalent to $\Delta R/R(H = H_{sat}) = 25\%$ at $H_{sat} = 10$ kOe). These amplitudes are larger than those for sputtered Co–Ag [3] in which pure Co is used instead of $Co_{70}Fe_{30}$. The same trend has been previously observed in magnetic multilayers [15] for which $Co_{90}Fe_{10}$/Cu multilayers exhibit a larger MR than Co/Cu multilayers. It seems, however, to depend on the conditions of preparation of the samples [19]. The observed increase in the magnetoresistance of $(Co_{70}Fe_{30})_xAg_{1-x}$ granular alloys may be due to an enhancement of the bulk spin-dependent scattering within the Co magnetic particles by the introduction of a small amount of Fe in the volume of these particles.

Figure 11 represents the initial slope $\partial(\Delta R/R)/\partial H|_{H=0}$ of the MR curve measured at RT versus annealing temperature for the same sample as in figure 10. A maximum slope of 18% kOe^{-1} has been obtained after annealing at 700 K. It is interesting to note that the annealing temperature which gives the largest slope is not the same as the optimal temperature for the largest MR amplitude (600 K). this difference comes from the different behaviours of the MR amplitude and the saturation field upon annealing.

Figure 12 shows the variation with temperature in the MR of a sample of composition $(Co_{70}Fe_{30})_{36}Ag_{64}$ after optimized annealing at 600 K for 10 min. The MR increases quite significantly as the temperature is decreased. As discussed in detail in [12] in regard to the $(Ni_{80}Fe_{20})_xAg_{1-x}$ series, there are two main origins of the MR in granular alloys: the GMR which originates from the spin-dependent scattering of conduction electrons at the interfaces or in the bulk of the magnetic grains, and the scattering of paramagnetic or superparamagnetic fluctuations. As the temperature is decreased, the former contribution increases, leading to the steeper and steeper MR slopes observed in low fields. This increase is mainly due to the decrease at low temperatures in the spin-flip scattering of conduction electrons caused by paramagnetic fluctuations. On the other hand, the scattering by magnetic fluctuations, which leads to the long MR tails observed at large fields, decreases at low temperature owing to the decrease in the density of these fluctuations.

The MR amplitude that we have obtained in these series of alloys is among the largest reported so far at 20 kOe [2] and 4 K ($\Delta R/R(H = 0) = 0.44$ equivalent to $\Delta R/R(H = 20\text{ kOe}) = 0.75$).

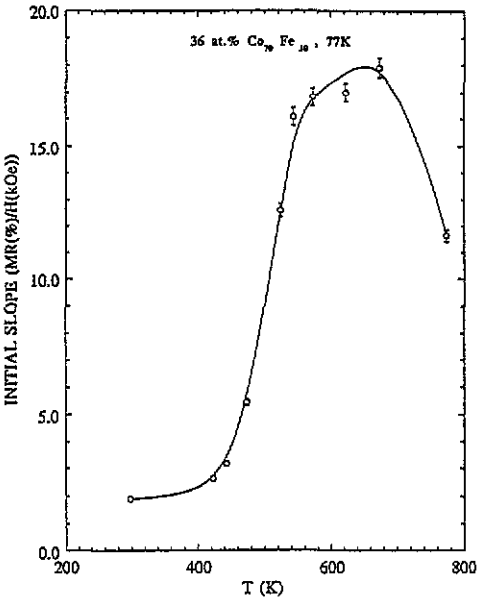

Figure 11. Initial slope of the MR *curve at* RT *for a sample of the composition* $(Co_{70}Fe_{30})_{36}Ag_{64}$ *after successive anneals for 10 min at various temperatures (derived from the same data as figure 9).*

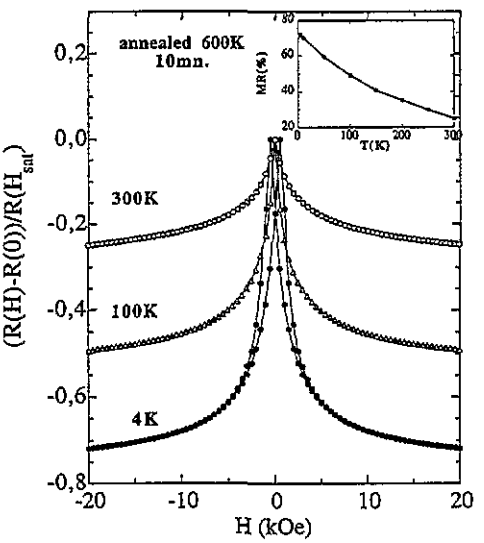

Figure 12. MR *curves measured at various temperatures between* ±20 kOe *for a sample of the composition* $(Co_{70}Fe_{30})_{36}Ag_{64}$ *after annealing for 10 min at 600 K. The inset shows the thermal variation in the amplitude of the* MR.

4. Conclusions

We have investigated the structural, magnetic and transport properties of the $(Co_{70}Fe_{30})_xAg_{1-x}$ series of granular alloys. Several original features have been found in these alloys in comparison with other previously studied series such as Co_xCu_{1-x} or $NiFe_xAg_{1-x}$. The magnetic precipitates are clearly more compact in the as-deposited and annealed samples than in the other series listed above. Up to 36 at.% of $Co_{70}Fe_{30}$ can be introduced into the Ag matrix before creating magnetic bridges between particles (compared with 25 at.% $NiFe_x$ particles in Ag). Upon moderate annealing, the superparamagnetic contribution to the magnetization increases (associated with round magnetic precipitates in annealed samples). Quite large MR amplitudes ($\Delta R/R(H=0) = 0.20$ at 10 kOe) and MR slopes ($\partial(\Delta R/R)/\partial H|_{H=0} \simeq 18\%$ kOe^{-1}) have been obtained in these series of alloys at RT.

Acknowledgments

We are very grateful to A Pierrot for his assistance with the sample preparation and to B Rodmacq and P Gerard for valuable discussions. One of us (SRT) wishes to thank the CNPq Conselho Nacional de Desenvolvimento Científico e Tecnológico, Brasil, for a fellowship.

References

[1] Berkowitz A, Young A P, Mitchell J R, Zang S, Carey M J, Spada F E, Parker F T, Hutten A and Thomas G 1992 *Phys. Rev. Lett.* **68** 3745

[2] Xiao J G, Jiang J S and Chien C L 1992 *Phys. Rev. Lett.* **68** 3749; 1993 *Proc. Intermag 93* paper HA03; 1993 *J. Appl. Phys.* **73** 5309
[3] Carey M J, Young A P, Stair A, Rao D and Berkowitz A E 1992 *Appl. Phys. Lett.* **61** 2935
[4] Tsoukatos A, Wan H, Hadjipanayis G C and Li Z G 1992 *Appl. Phys. Lett.* **61** 2362
[5] Xiong P, Xiao G, Wang J G, Xiao J G, Jiang J S and Chien C L 1992 *Phys. Rev. Lett.* **69** 3220
[6] Parkin S S P, Farrow R F C, Rabedeau T A and Marks R F 1993 *Europhys. Lett.* **22** 455
[7] Watson M L, Barnard J A, Hossain S and Parker M R 1993 *J. Appl. Phys.* **73** 5506
[8] Thompson S M, Gregg J F, Staddon C R, Daniel D, Dawson S J, Ounadjela K, Hammann J, Fermon C, Saux G, O'Grady K, Grieves S J, Coey J M D and Fagan A 1993 *Phil. Mag.* B **68** 923
[9] Lodder J C, de Haan P and Van Kranenburg H 1993 *J. Magn. Magn. Mater.* **128** 219
[10] Xiao G, Wang J Q and Xiong P 1993 *Proc. Intermag 93* paper HA04
[11] Chien C L, Xiao J Q and Jiang S 1993 *J. Appl. Phys.* **73** 5309
[12] Dieny B, Teixeira S R, Rodmacq B, Cowache C, Auffret S, Redon O and Pierre J 1994 *J. Magn. Magn. Mater.* **130** 197
[13] Pratt W P Jr, Lee S F, Slaughter J M, Loloee R, Schroeder P A and Bass J 1991 *Phys. Rev. Lett.* **66** 3060; Lee S F, Pratt W P, Loloee R, Schroeder P A and Bass J 1992 *Phys. Rev.* B **46** 548
[14] Hylton T L, Coffey K R, Parker M A and Howard J K 1993 *Science* **261** 1021
[15] Inomata K and Saito Y 1993 *J. Magn. Magn. Mater.* **126** 425
[16] Vincze I, Campbell I A and Meyer A J 1974 *Solid State Commun.* **15** 1495
[17] Chappert C, Dang K Le, Beauvillain P, Hurdequint H and Renard D 1986 *Phys. Rev.* B **34** 3192
[18] Massalski T B, Murray J L, Bennett L H and Baker H (ed) 1986 *Binary Alloy Phase Diagrams* (Metals Park, OH: American Society for Metals)
[19] Coehoorn R and Duchateau J P W B 1993 *J. Magn. Magn. Mater.* **126** 390